Copper Reduction by the Octapeptide Repeat Region of Prion Protein: pH Dependence and Implications in Cellular Copper Uptake†

Takashi Miura, Satoshi Sasaki, Akira Toyama, and Hideo Takeuchi*

Graduate School of Pharmaceutical Sciences, Tohoku University, Aobayama, Sendai 980-8578, Japan

Received January 29, 2005; Revised Manuscript Received March 31, 2005

ABSTRACT: The physiological function of the prion protein (PrP) remains enigmatic despite its established involvement in the pathogenesis of spongiform encephalopathies. PrP is a glycolipid-anchored membrane protein, which constitutively recycles between the cell surface and an endosomal compartment. The N-terminal region of PrP contains a four tandem repeat (OP4) of the octapeptide PHGGGWGQ (OP) that binds and reduces Cu(II) ions. We have examined the kinetic properties of the OP4-mediated Cu(II) reduction and found that OP4 exhibits the highest reduction activity around pH 6.5, close to the pH in early endosomes. All four OP units and at least one tryptophan side chain are essential for Cu(II) reduction. The reaction is described by an uncompetitive substrate inhibition mechanism involving a 1:1 Cu(II)−OP4 active intermediate. Structural analysis by Raman spectroscopy has revealed that the Cu(II) ion is coordinated by four histidine Nτ atoms in the active intermediate and the feasibility of formation of this intermediate correlates with the Cu(II) reduction over a pH range from 5.0 to 8.2. Molecular mechanics calculations suggest that two tryptophan residues of OP4 are located near the Cu(II) site, being consistent with the importance of redox-active tryptophan in the Cu(II) reduction. PrP has been proposed to capture Cu(II) ions in the extracellular space and release them in the endosome. The results of this study strongly suggest that PrP also plays a role in the reduction of captured Cu(II) ions prior to their transfer to Cu(I)-specific intracellular copper trafficking proteins.

The prion protein (PrP)[1] is a synaptic glycoprotein attached to the neuronal cell surface via a glycosylphosphatidylinositol anchor (*1*−*3*). Human PrP after posttranslational modification comprises 209 amino acids (residues 23−231), which are highly conserved among mammals (*4*, *5*). The N-terminal half of the PrP polypeptide chain is largely unstructured, while the C-terminal half is folded into a globular structure containing three α-helices and two short β-strands (*6*−*9*). The normal cellular form of PrP is converted to a β-sheet-rich pathogenic isoform, and deposition of the protease-resistant pathogenic isoform in the central nervous system is considered to be the key event in the development of fatal neurodegenerative disorders such as Creutzfeldt−Jakob disease in humans and spongiform encephalopathy in animals (*1*, *10*, *11*). Despite the progress made in understanding the prion biology and pathology, the physiological function of PrP still remains unclear.

Several experimental findings suggest that PrP plays a role in copper uptake from extracellular environments (*12*−*16*). The Cu(II) ion was reported to stimulate endocytosis of PrP, which constitutively recycles between the plasma membrane and early endosomes in neuronal cells (*12*−*14*). In PrP gene-ablated mice, a significant decrease in copper content was observed for synaptosome- and endosome-enriched subcellular fractions of the brain (*15*). An analogous decrease of synaptosomal copper content was also caused by deletion of residues 32−93 from the mouse PrP polypeptide chain (*16*). The deleted peptide segment includes a stretch (residues 60−91) of four sequential copies of the octapeptide sequence Pro-His-Gly-Gly-Gly-Trp-Gly-Gln (PHGGGWGQ), which is known to bind Cu(II) ions preferentially over other metal ions (*17*, *18*). Since the octapeptide repeat region of PrP is highly conserved in mammals (*4*, *5*), its specific affinity for Cu(II) is considered to be of physiological relevance.

The Cu(II) binding mode of the prion octapeptide repeat region has been studied extensively by using various analytical methods including Raman spectroscopy, electron spin resonance (ESR), and mass spectrometry (*19*−*27*). Most analytical studies showed that the octapeptide unit PHGGGWGQ (OP) binds one Cu(II) ion at pH 7.4−8.0 with an apparent dissociation constant in the low micromolar range (*20*−*25*). Raman spectra further demonstrated that a Cu(II) ion is chelated by the imidazole Nπ atom of histidine and two main-chain amide nitrogens of the OP unit (*20*). An analogous chelation was later found by X-ray diffraction in the Cu(II) complex of HGGGW, which spans the central region of OP (*28*). Mass spectrometry and ESR studies confirmed that PrP fragments containing a four tandem repeat

† This work was supported in part by a Grant-in-Aid for Scientific Research (15590037) from the Ministry of Education, Culture, Sports, Science, and Technology of Japan and by a grant from the Sumitomo Foundation.

* Corresponding author. Phone/Fax: +81-22-795-6855. E-mail: takeuchi@mail.tains.tohoku.ac.jp.

[1] Abbreviations: BC, bathocuproinedisulfonic acid; Ctr1, copper transporter 1; ESR, electron spin resonance; MES, 2-morpholineethanesulfonic acid; OP, prion octapeptide repeating unit PHGGGWGQ; OP*n*, peptide consisting of an *n* tandem repeat of OP ($n = 1-4$); OP4(W→A), mutant of OP4 with all tryptophan residues being replaced by Ala; PrP, prion protein; *R*, molar ratio of Cu(II) to OP4 or OP4(W→A).

10.1021/bi0501784 CCC: $30.25
Published on Web 05/18/2005

of OP (OP4) can bind four Cu(II) ions at pH 7.4 (*22*, *23*, *28*).

Upon acidification to pH ~6, the Cu(II) affinity of the octapeptide repeat region drastically decreases (*18*, *22*). Concomitantly, the Cu(II)−amide linkages observed at neutral pH are broken, and the Cu(II) binding site on the histidine imidazole ring changes from Nπ to Nτ (*20*). The pH-sensitive Cu(II) binding mode, taken together with the endocytic recycling of PrP (*12*−*14*), leads to the proposal that PrP acquires Cu(II) ions from the extracellular medium at neutral pH and releases the captured ions in the acidic endosomal compartment, thus transporting Cu(II) ions from the extracellular to intracellular space through endocytosis of the protein itself (*12*−*14*, *20*, *22*, *28*). Since monovalent Cu(I) is the ion that is bound and delivered by copper chaperones to target proteins in the cytoplasm (*29*, *30*), the endocytosed divalent Cu(II) ions need to be reduced to Cu(I) in order to be used efficiently in the cytoplasm. Recently, Ruiz et al. have reported that the octapeptide repeat region has an ability to reduce the Cu(II) ion to Cu(I) at pH 7.4 (*31*), though it remains to be assessed whether the octapeptide repeat region has a Cu(II)-reducing ability even under acidic conditions such as in the endosomal compartment.

In this study, we have examined the Cu(II) reduction of peptides comprising 1−4 OP repeating units (OP1−OP4) in a pH range from 5.0 to 8.2. The result clearly shows that the four tandem repeat of OP is essential for Cu(II) reduction and the Cu(II) reduction activity of OP4 is highest at mildly acidic pH. Structural analysis by Raman spectroscopy has further demonstrated that the active reaction intermediate is a 1:1 Cu(II)−OP4 complex, in which the Cu(II) ion is coordinated by four histidine Nτ atoms. These observations strongly suggest that the octapeptide repeat region of PrP is involved not only in the Cu(II) transport from the extracellular medium to an endosome but also in the reduction of the captured Cu(II) ions to efficiently pass them to Cu(I)-specific intracellular copper trafficking proteins.

MATERIALS AND METHODS

Preparation of Peptides. Peptides composed of *n* (n = 1−4) sequential copies of the prion octapeptide $(PHGGGWGQ)_n$ (OP*n*) were synthesized on an Applied Biosystems Model 431A automated peptide synthesizer by using the 9-fluorenylmethoxycarbonyl method. A Trp → Ala mutant of OP4 [$(PHGGGAGQ)_4$, OP4(W→A)] was also synthesized in the same way. The N-terminus of each peptide was acetylated in order to avoid deprotonation and metal coordination at the Pro imino nitrogen. Cleavage of the peptide from the resin and removal of the protecting groups were performed in a mixture of 10 mL of trifluoroacetic acid, 0.75 g of phenol, 0.25 mL of 1,2-ethanedithiol, 0.5 mL of thioanisole, and 0.5 mL of water for OP*n* or in a mixture of 9.5 mL of trifluoroacetic acid, 0.25 mL of 1,2-ethanedithiol, and 0.25 mL of water for OP4(W→A). The crude peptide was purified by HPLC on a reversed-phase column (Cosmosil $5C_{18}$-AR, Nacalai Tesque) by using a 0−40% linear gradient of acetonitrile in 0.1% (v/v) trifluoroacetic acid. Lyophilized powder of the purified peptide was dissolved in 100 mM hydrochloric acid and again lyophilized to remove residual trifluoroacetic acid. The concentration of OP1−OP4 was determined by using the 280 nm absorption intensity of the tryptophan residue (ϵ_{280} = 5460 M^{-1} cm^{-1}). For OP4(W→A), the peptide concentration was measured by using the relative intensity of an N-deuterated histidine Raman band at 1408 cm^{-1} against a water (D_2O) Raman band at 1204 cm^{-1} in acidic D_2O solution. Then, the D_2O solution was lyophilized, and the peptide was dissolved in H_2O (or in buffer) at desired concentrations. For Raman spectral samples of OP4(W→A), buffer was not used to avoid possible spectral interference, and the pH of the solution was adjusted by using HCl and NaOH.

Kinetic Assays of Cu(II) Reduction. The Cu(II) reduction by OP1−OP4 and by the mutant OP4(W→A) was assayed with a Cu(I)-specific chelator, bathocuproinedisulfonic acid (BC, Nacalai Tesque). BC forms a Cu(I)−BC_2 complex and exhibits a characteristic absorption band at 483 nm (*31*−*33*). In a typical protocol, the reaction was monitored at room temperature in a 1 cm quartz optical cell, which contained 20 μM Cu(II)−Gly_2 (a 1:2 mixture of $CuCl_2$ and glycine), 25/*n* μM OP*n* (n = 1−4, 25 μM in OP unit irrespective of *n*), and 360 μM BC. The absorbance at 483 nm at a given time of reaction was converted into the concentration of Cu(I) by using the molar extinction coefficient, 12250 M^{-1} cm^{-1}, of the Cu(I)−BC_2 complex (*34*). The concentration of Cu(I) was recorded at a 5 s interval within the 10−60 s time range after addition of Cu(II). Cu(II)−Gly_2 was employed as a source of Cu(II) to minimize the turbidity due to the formation of insoluble metal−hydroxy and metal−oxy polymers by free Cu(II) ions at neutral-to-alkaline pH (*15*). The buffer used for preparation of the reaction mixtures was 18 mM 2-morpholineethanesulfonic acid (MES) (pH 5.0−6.8) or sodium phosphate (pH 6.0−8.2) supplemented with 135 mM NaCl. In the overlapping pH region (pH 6.0−6.8), the kinetic data obtained in the two buffers were averaged. When ascorbic acid, a common reductant in enzymatic reactions, was used instead of the peptides, the absorbance at 483 nm rapidly reached a plateau irrespective of the solution pH, confirming that the affinity of BC for Cu(I) and the molar extinction coefficient of the Cu(I)−BC_2 complex are not affected by the solution pH, at least in the pH range (5.0−8.2) examined here.

Raman Spectroscopy. Raman spectra were recorded for aqueous solutions containing 10 mM OP4(W→A) and varied amounts of $CuCl_2$ at pH 5.0−8.2. The sample solution was sealed in a glass capillary tube and excited with the 514.5 nm line (40 mW at the sample) of a Coherent Innova 70 Ar^+ laser. The scattered light was collected with a camera lens and dispersed on a Jasco NR-1800 triple spectrometer equipped with a liquid nitrogen-cooled CCD detector. The intensities of Raman spectra were normalized by using the C−H deformation band at 1455 cm^{-1}. The solvent H_2O Raman band at 1640 cm^{-1} was subtracted after the intensity normalization.

Molecular Modeling. An initial structure of the 1:1 Cu(II)−OP4 complex was generated by the Biopolymer module of Insight II 2000/Discover (Accelrys), and energy minimization was repeated until the root-mean-square gradient fell below 0.1 kcal mol^{-1} $Å^{-1}$. Then, simulated annealing was performed by heating the energy-minimized structure to 900 K for 5 ps, cooling to 300 K over 10 ps, and equilibrating at 300 K for 8 ps (*35*). During the simulated annealing process, all of the peptide bonds were constrained to be *trans* to avoid isomerization to *cis* bonds. Each of the

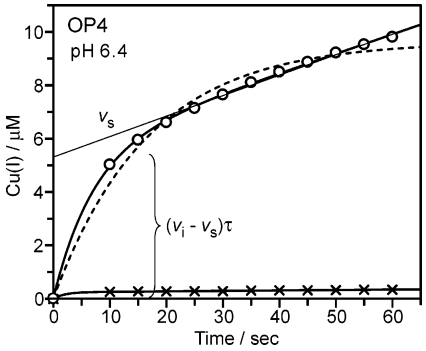

FIGURE 1: Progress curve of the OP4-mediated Cu(II) reduction. The concentration of Cu(I) produced is plotted against the time after mixing of 20 μM Cu(II) and 6.25 μM OP4 in the presence of 360 μM BC at pH 6.4. The buffer used was 18 mM MES supplemented with 135 mM NaCl. The concentration of Cu(I) (circles) was determined by using a 483 nm visible absorption band of the Cu(I)−BC_2 complex ($\epsilon_{483} = 12250\ M^{-1}\ cm^{-1}$). The broken curve shows a trial fit of the experimental data with a single exponential function representing a simple first-order kinetics. The solid curve shows the least-squares fit of the experimental data to a biphasic progress curve described by eq 1. The slope of the straight line at $t \geq 25$ s gives the steady-state velocity v_s, and the intercept of the straight line at $t = 0$ corresponds to the concentration of Cu(I) produced in the initial burst phase, $(v_i - v_s)\tau$. The points marked with a cross represent the control data in the absence of OP4.

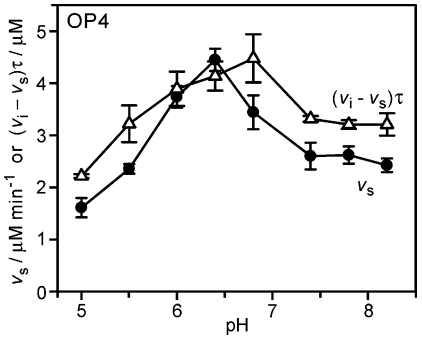

FIGURE 2: pH dependence of the steady-state velocity v_s (triangle) and of the concentration of Cu(I) produced in the initial burst phase, $(v_i - v_s)\tau$ (filled circle), in the Cu(II) reduction reaction by OP4. Each data point represents the mean ± SD of three to six independent measurements. The assays were performed at 6.25 μM OP4 and 360 μM BC in 18 mM MES (pH 5.0−6.8) or phosphate buffer (pH 6.0−8.2) supplemented with 135 mM NaCl. The initial Cu(II) concentration was 20 μM. The data shown in the pH 6.0−6.8 region are averages of the values measured in the MES and phosphate buffers.

100 structures generated by repetitive simulated annealing was solvated using a 5 Å H_2O shell and then energy minimized to a root-mean-square gradient of 0.1 kcal mol^{-1} $Å^{-1}$. A few series of simulated annealing and energy minimization were started from different initial structures. The lowest energy structure obtained was selected as the most probable model. In molecular dynamics calculations, a time step of 1 fs was used. The Discover3 software package with the ESFF force field was used throughout the modeling (*36*). All calculations were performed on a Power Indigo2 workstation (Silicon Graphics).

RESULTS

Cu(II) Reduction by OP4. Figure 1 shows a plot of the Cu(I) concentration against the time after mixing of 20 μM Cu(II) and 6.25 μM OP4 in the presence of 360 μM BC at pH 6.4. The control data recorded in the absence of OP4 (marked with a cross) indicate that the Cu(II) reduction is exclusively due to the peptide. The progress curve of OP4-mediated Cu(II) reduction cannot be fitted with a single exponential function representing a simple first-order kinetics as indicated with the broken line in the figure. Close examination of the progress curve reveals an initial burst of Cu(I) production followed by a slower and linear accumulation of Cu(I). These features of the progress curve suggest that the Cu(II) reduction by OP4 is described as a biphasic reaction, in which the rate of product formation (v) decays from an initial high value (v_i) to a steady-state low value (v_s) with an exponential time constant (τ) as given in the equation (*37*, *38*):

$$v = v_s + (v_i - v_s)\exp(-t/\tau) \qquad (1)$$

Here, t stands for the time after mixing of the reactants. Integration of eq 1 provides an expression for the time dependence of the Cu(I) concentration:

$$[\mathrm{Cu(I)}] = v_s t + (v_i - v_s)\tau\{1 - \exp(-t/\tau)\} \qquad (2)$$

The solid curve in Figure 1 shows the result of least-squares fitting of the experimental progress curve to eq 2. The good fit between experiment and calculation lends support to the biphasic reaction model. Graphically, the slope of the progress curve in the steady state (at $t > 25$ s) represents the linear coefficient v_s, and the vertical intercept of the v_s straight line extrapolated to $t = 0$ corresponds to the exponential coefficient $(v_i - v_s)\tau$, which represents the amount of Cu(I) produced in the initial burst phase. Both v_s and $(v_i - v_s)\tau$ characterize the biphasic reaction and reflect the Cu(II) reduction activity of OP4.

pH Dependence of Cu(II) Reduction. The Cu(II) reduction by OP4 was examined in the pH 5.0−8.2 range. The v_s and $(v_i - v_s)\tau$ values obtained are plotted as a function of pH in Figure 2, which demonstrates that the optimum pH for the Cu(II) reduction is around 6.5 in both the steady state and the burst phase. At pH 5, v_s drops to about one-third that at pH 6.5, while it decreases to about one-half at pH ≥7.4. An analogous change with pH is seen for $(v_i - v_s)\tau$. These observations imply that there are at least two factors that decrease the Cu(II) reduction activity of OP4, one effective at strongly acidic pH and the other at neutral-to-alkaline pH. As a compromise of these two opposing factors, OP4 acquires the highest activity of Cu(II) reduction at mildly acidic pH. Since v_s and $(v_i - v_s)\tau$ exhibit similar pH dependence and the steady state lasts much longer than the burst phase, we will hereafter use the steady-state velocity v_s as a measure of Cu(II) reduction activity of OP4 and related peptides.

Structural Elements Necessary for Cu(II) Reduction. OP4 comprises four OP units and shows a significant Cu(II) reduction activity as described above. To test whether shorter peptides have similar properties, we performed Cu(II) reduction assays on peptides consisting of one, two, and three OP units, i.e., OP1, OP2, and OP3. In the assays, the concentrations of OP1, OP2, and OP3 were set to be 25, 12.5, and 8.33 μM, respectively, in order not to change the molar ratio of the Cu(II)/OP unit from that in the previous

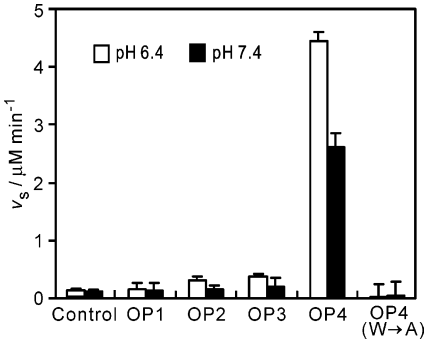

FIGURE 3: Comparison of the Cu(II) reduction steady-state velocity v_s for control (in the absence of peptide), OP1, OP2, OP3, OP4, and OP4(W→A) at pH 6.4 (MES buffer) and 7.4 (phosphate buffer). Data points represent means ± SD ($n = 3$). The concentrations of OP1, OP2, OP3, OP4, and OP4(W→A) were 25, 12.5, 8.33, 6.25, and 6.25 μM. The other solution conditions were the same as in Figure 2.

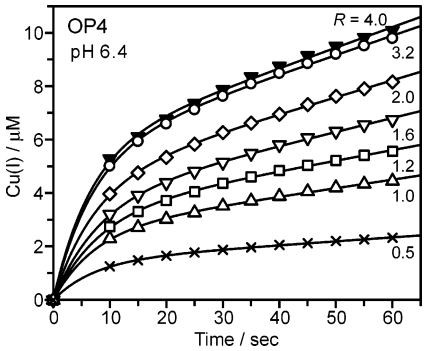

FIGURE 4: Effects of the initial Cu(II) concentration on the progress curve of Cu(II) reduction by OP4 at pH 6.4 (MES buffer). The value of R in the figure stands for the Cu(II)/OP4 molar ratio. The concentration of OP4 was 6.25 μM, and the initial concentration of Cu(II) was varied from 3.125 to 25 μM. The other solution conditions were the same as in Figure 2.

OP4 assays. Figure 3 compares the v_s values of these shorter peptides at pH 6.4 and 7.4 with those of OP4 and in the absence of peptide. None of the shorter peptides reduces Cu(II) ions significantly, demonstrating that the tandem repeat of four OP units is essential for Cu(II) reduction.

Ruiz et al. reported that the replacement of four tryptophan residues of OP4 with Ala largely diminishes the amount of Cu(II) reduced in a 60 min incubation at pH 7.4 (*31*). We examined the time course of Cu(II) reduction by the Trp → Ala mutant, OP4(W→A), at both pH 6.4 and pH 7.4. The v_s values obtained for OP4(W→A) are compared with those of wild-type OP4 in Figure 3. The mutation almost destroys the Cu(II)-reducing ability of OP4, indicating that at least one of the four tryptophan residues in OP4 plays a crucial role in Cu(II) reduction. Tryptophan is a well-known redox-active amino acid, and the indole ring on its side chain is expected to act as an electron donor to Cu(II) (*39*, *40*). The lack of an electron donor in OP4(W→A) may be the reason this mutant fails to reduce Cu(II) ions.

Active Species. In the Cu(II) reduction assays described above, the initial molar ratio of Cu(II) to OP4 (R) was fixed at 3.2. We have examined the effect of R on the Cu(II) reduction at pH 6.4. Figure 4 shows the progress curves at different R values ranging from 0.5 to 4, i.e., 3.125−25 μM Cu(II) against 6.25 μM OP4. As shown with solid curves in Figure 4, the progress curve is well reproduced by eq 2 at

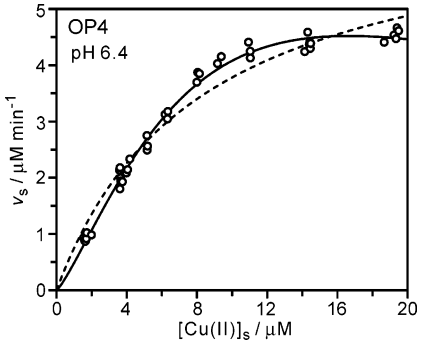

FIGURE 5: Plot of the steady-state velocity v_s against the steady-state Cu(II) concentration $[Cu(II)]_s$ at pH 6.4 (MES buffer). The data points (circles) were obtained by assays at 40 different Cu(II) concentrations in the presence of 6.25 μM OP4. The other solution conditions employed in the assays were the same as in Figure 2. The broken curve shows a fit of the experimental data with a Michaelis−Menten equation, while the solid curve is a fit to the uncompetitive substrate inhibition model described by eqs 3−5.

every R value, suggesting that the reaction is governed by a common mechanism irrespective of R. The change in R is reflected in both v_s (the slope of the straight progress line at $t > 25$ s) and $(v_i - v_s)\tau$ (the vertical intercept of the straight v_s line). In enzyme kinetic studies, the steady-state velocity is sometimes plotted against the substrate concentration to get insight into the reaction mechanism. In the present case, however, a plot of v_s against the initial concentration of Cu(II) is not appropriate because a significant fraction of Cu(II) is readily converted to Cu(I) in the initial burst phase. The Cu(II) concentration in the steady state $[Cu(II)]_s$ is estimated by subtracting the concentration of Cu(II) reduced in the burst phase $[(v_i - v_s)\tau]$ from the initial Cu(II) concentration. The $[Cu(II)]_s$ value thus obtained may be applicable throughout the steady state because the Cu(II) → Cu(I) change proceeds slowly in the steady state.

Figure 5 shows a plot of v_s as a function of $[Cu(II)]_s$ at pH 6.4. The values of v_s and $[Cu(II)]_s$ were obtained by analyzing 40 progress curves observed at varied Cu(II) concentrations. The v_s value increases with increase of $[Cu(II)]_s$ at low concentrations of Cu(II). At high concentrations of Cu(II), however, the velocity rapidly decreases, and the plot deviates from the usual hyperbolic saturation curve (broken line in Figure 5) of the Michaelis−Menten equation (*41*). Such unusual behavior of v_s may be explained by an uncompetitive substrate inhibition model (*42*, *43*):

$$n\mathrm{Cu(II)} + \mathrm{OP4} \overset{K_m}{\rightleftharpoons} \mathrm{Cu(II)}_n\text{−OP4} \overset{k}{\rightarrow} n\mathrm{Cu(I)} + \mathrm{OP4} \quad (3)$$

$$\mathrm{Cu(II)}_n\text{−OP4} + \mathrm{Cu(II)} \overset{K_i}{\rightleftharpoons} \mathrm{Cu(II)}_{n+1}\text{−OP4} \quad (4)$$

Here, n is the number of active Cu(II) binding sites per molecule of OP4 and k is the rate constant. K_m and K_i are the dissociation constants of the active intermediate $Cu(II)_n$-OP4 and the inactive complex $Cu(II)_{n+1}$−OP4, respectively. In this model, the reaction velocity is given by the equation (*42*, *43*):

$$v_s = nk[\mathrm{OP4}]_0[\mathrm{Cu(II)}]_s^n/\{K_m + [\mathrm{Cu(II)}]_s^n + [\mathrm{Cu(II)}]_s^{n+1}/K_i\} \quad (5)$$

where $[OP4]_0$ is the concentration of OP4 (6.25 μM). [The Michaelis−Menten equation is given by setting $n = 1$ and $K_i = \infty$ in eq 5.] Nonlinear least-squares fitting of eq 5 to the data plotted in Figure 5 provides the parameter values $n = 1.2 \pm 0.1$, $k = 1.7 \pm 1.0$ min^{-1}, $K_m = 25 \pm 11$ μM, and $K_i = 17 \pm 13$ μM. The calculated saturation curve (solid line in Figure 5) is in good agreement with the experimental data (circles). The value of n is close to unity, indicating that Cu(II) is reduced through a 1:1 Cu(II)−OP4 intermediate. Additional binding of a Cu(II) ion to the reaction intermediate leads to the formation of a 2:1 $Cu(II)_2$−OP4 complex, which is inactive in Cu(II) reduction. Possibly, Cu(II) ions further bind to the inactive complex, though such multiple binding is not explicitly incorporated in the model described above. In any case, formation of inactive complexes will decrease the apparent value of v_s. As shown in Figure 2, the v_s value decreases at pH 7.4 compared to that at pH 6.4. Analysis of the v_s−$[Cu(II)]_s$ relationship at pH 7.4 gave a value of K_i (~6 μM; data not shown) which is smaller than that at pH 6.4 and indicative of an increased formation of inactive complexes. The Cu(II) reduction activity of OP4 may be linked with the feasibility of formation of the active 1:1 Cu(II)−OP4 complex. Raman spectra provide the evidence for the formation of a 1:1 Cu(II)−OP4 complex (vide infra).

Cu(II) Coordination in the Active Intermediate. The kinetic data reported above have shown that the 1:1 Cu(II)−OP4 complex plays a key role as an active intermediate in the Cu(II) reduction. To understand the mechanism of the Cu(II) reduction, the structure of the intermediate is very important. However, in usual cases, reaction intermediates are so short-lived and poorly populated that their structures are difficult to study without the use of special techniques such as time-resolved detection synchronized with initiation of the reaction or chemical modification that stops the reaction at a selected intermediate state. In this study, we have employed the Trp → Ala mutation to capture the intermediate. The OP4(W→A) mutant lacks the tryptophan side chains essential for Cu(II) reduction but retains histidine side chains and the main-chain amide groups that can be involved in direct interaction with Cu(II) (*20*). Therefore, the Cu(II)−peptide interaction is unlikely to be affected by the Trp → Ala mutation, and the OP4(W→A) mutant is expected to serve as an appropriate model for studying the Cu(II) binding mode of OP4 in the reaction pathway of Cu(II) reduction.

The interaction between Cu(II) and OP4(W→A) was examined by Raman spectroscopy, which is a useful tool for studying metal binding modes of histidine residues (*19*, *20*, *44*, *45*). Figure 6 shows the Raman spectra of aqueous mixtures of Cu(II) and OP4(W→A) with metal/peptide molar ratios (R) of 0−4.0 at pH 6.4, where OP4 exhibited the highest Cu(II) reduction activity. The 1574 cm^{-1} band in the spectrum of the metal-free solution ($R = 0$, Figure 6A) is assignable to the C_4═C_5 stretch mode of imidazole side chains of four histidine residues in OP4 (one each from individual OP units) (*46*). The wavenumber of the C_4═C_5 stretch band is known to be sensitive to the protonation and metal binding states at two imidazole nitrogens (Nπ and Nτ) (*45*−*49*). The corresponding band of histidinium (His^+, both Nπ and Nτ being protonated) is observed at 1635 cm^{-1}, indicating that the histidine residues are partially converted to His^+ at pH 6.4 in the metal-free solution. In the presence

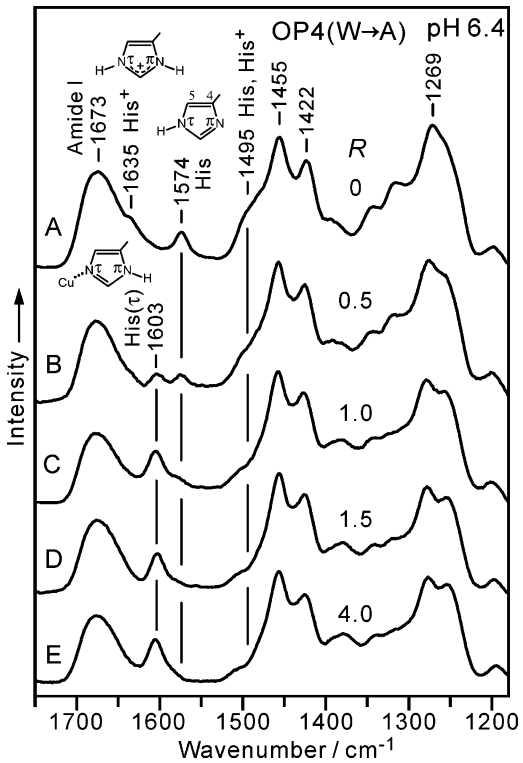

FIGURE 6: Raman spectra of OP4(W→A) (10 mM, pH 6.4) in the absence and presence of Cu(II). The Cu(II)/peptide molar ratio (R) was varied from 0 (A) to 4.0 (E). The Raman bands assignable to neutral histidine (His), cationic histidine (His^+), Nτ-Cu(II) coordinated histidine [His(τ)], and the amide I mode of the peptide main chain are indicated with corresponding labels. The 1455 cm^{-1} band is due to C−H bend vibrations and is used as an internal intensity reference. The bands at 1422 and 1269 cm^{-1} are ascribed to overlaps of multiple bands arising from glutamine, histidine, and the peptide main chain.

of Cu(II) at $R = 0.5$, both the 1574 and 1635 cm^{-1} bands decrease in intensity (Figure 6B). A broad shoulder at 1495 cm^{-1} arising from His and His^+ also loses intensity. Concomitantly, a new band appears at 1603 cm^{-1}, which is assignable to the C_4═C_5 stretch of histidine bound to Cu(II) through Nτ [His(τ)] (*45*, *47*−*49*). At $R = 1.0$, the 1635, 1574, and 1495 cm^{-1} bands almost disappear, and the 1603 cm^{-1} band of His(τ) becomes dominant in the 1650−1550 cm^{-1} region (Figure 6C). As Figure 6D shows, the Raman spectral change is already completed at $R = 1.5$, indicating that OP4 complexes containing more than one Cu(II) ion, if any, are not populated significantly and the dominant species in the solution is the 1:1 metal−peptide complex suggested by the analysis of kinetic data. The Raman spectrum exhibits no further change even when R is increased to 4.0 (Figure 6E). These observations indicate that only the Nτ−Cu(II) coordination is possible at pH 6.4 and all four histidine Nτ atoms of a OP4(W→A) molecule are bound to the same Cu(II) ion [Cu(II)−Nτ_4] in the 1:1 metal−peptide complex. The Cu(II) ion in the active intermediate of Cu(II)−OP4 may also be coordinated by histidine residues in the same way.

Structural Origin of the pH Dependence of Cu(II) Reduction. The Cu(II)-reducing ability of OP4 shows a significant pH dependence as shown in Figure 2. The origin of the pH dependence has also been investigated by using OP4(W→A) and Raman spectroscopy. Figure 7 shows the Raman spectra of a mixture of Cu(II) and OP4(W→A) at pH 5.0, 6.4, 7.4, and 8.2. The metal to peptide molar ratio R is 3.2, as in the

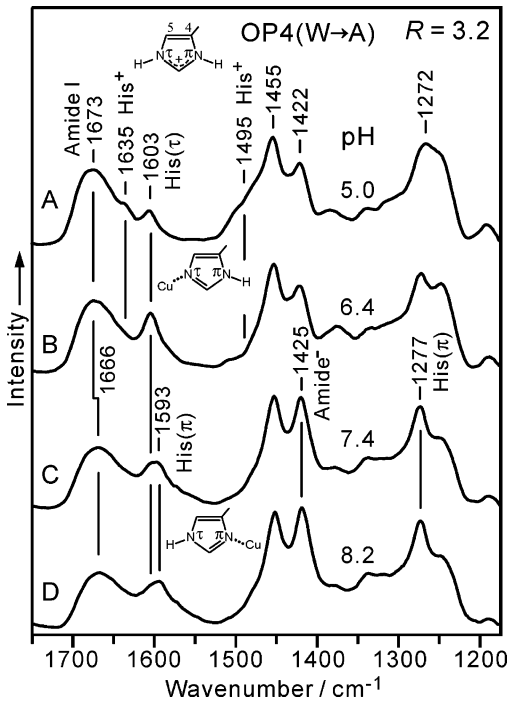

FIGURE 7: Effect of pH on the Raman spectrum of OP4(W→A) (10 mM) in the presence of Cu(II) ($R = 3.2$). The pH values were 5.0 (A), 6.4 (B), 7.4 (C), and 8.2 (D). The spectra exhibit the Raman bands due to cationic histidine (His^+), Nτ−Cu(II) coordinated histidine [His(τ)], Nπ−Cu(II) coordinated histidine [His(π)], deprotonated amide (amide$^-$), and the amide I mode of the peptide main chain as indicated. The 1455 cm^{-1} band is due to C−H bend vibrations and is used as an internal intensity reference. The bands at 1422 and 1272 cm^{-1} are ascribed to overlaps of multiple bands arising from glutamine, histidine, and the peptide main chain.

kinetic assays. In comparison with the Raman spectrum at pH 6.4 (Figure 7B), the 1603 cm^{-1} band of His(τ) is weak, and instead the 1635 cm^{-1} band of His^+ is more clearly seen in the spectrum at pH 5.0 (Figure 7A). These spectral features indicate that a significant fraction of histidine is fully protonated at pH 5.0 and is not available for Cu(II) binding. The conversion from neutral His to cationic His^+ must be responsible for the loss of Cu(II)-reducing ability at acidic pH.

When the pH of the solution is elevated from 6.4 to 7.4−8.2 (Figure 7C,D), the 1603 cm^{-1} band of His(τ) becomes weak and a new band grows at 1593 cm^{-1}. The 1593 cm^{-1} band is ascribed to the C_4═C_5 stretch mode of histidine with Nπ−Cu(II) coordination [His(π)] (*45*, *47*−*49*). The conversion of the Cu(II) binding site from Nτ to Nπ is supported by the appearance of a prominent band at 1277 cm^{-1}, which is also a marker of Nπ−metal coordination (*45*, *47*−*49*). In conjunction with the change in Cu(II)−histidine interaction, a significant intensity increase occurs at 1425 cm^{-1} (Figure 7C,D), which is ascribed to the C═O/C−N$^-$ stretching band of deprotonated and Cu(II)-bound main-chain amide (amide$^-$) (*50*). It is known that divalent metal ions such as Cu(II) are capable of inducing deprotonation and metal binding of the peptide amide nitrogen at neutral-to-alkaline pH (*51*). The weakening and small shift of the amide I band at ∼1670 cm^{-1} (Figure 7C,D) may be ascribed to a change in the main-chain vibrational mode due to the binding of Cu(II) to one or more amide nitrogens. The Raman spectra clearly demonstrate that Cu(II) ions are bound to histidine Nπ and main-chain amide nitrogen atoms [Cu(II)−(Nπ, amide$^-$)] at

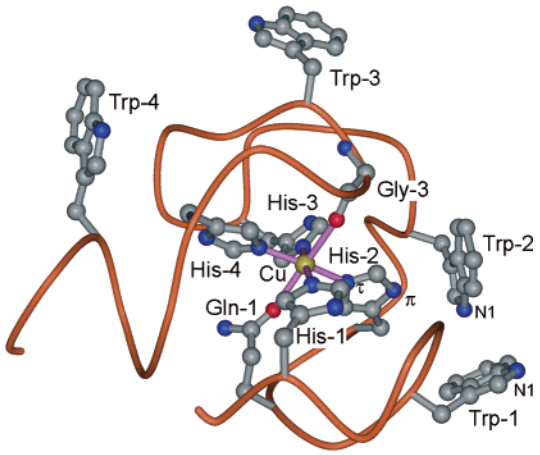

FIGURE 8: Model for the 1:1 Cu(II)−OP4 complex obtained by molecular mechanics calculations. The peptide main chain of OP4 is depicted as a string except for the most C-terminal glycine residue of the third OP unit (Gly-3). Side-chain atoms are shown only for tryptophan and Cu(II)−ligand amino acids for clarity. The number suffixed to the residue name represents the index of OP unit (1−4) to which the residue belongs.

pH ≥7.4. In a previous study, we showed that each octapeptide unit of OP4 could form a Cu(II)−(Nπ, amide$^-$)-type chelation at neutral-to-alkaline pH (*20*). If the Cu(II)−(Nπ, amide$^-$)-type chelation occurs in one or more OP units of an OP4 molecule, the OP4 molecule would become inactive in Cu(II) reduction because large structural rearrangements are needed to form the Cu(II)−Nτ_4-type active intermediate. The binding of Cu(II) to the main-chain amide followed by Cu(II)−(Nπ, amide$^-$) chelation is likely to be the cause of the decrease in Cu(II) reduction activity at pH ≥7.4.

Model Structure for the Active Intermediate. In addition to histidine residues, tryptophan residues also play a critical role in Cu(II) reduction as evidenced by the complete loss of reduction activity upon mutation of tryptophan to alanine (Figure 2). Since tryptophan is a redox-active amino acid (*39*, *40*), a plausible role of tryptophan is to donate an electron to the Cu(II) ion that is captured by the Cu(II)−Nτ_4-type coordination in the 1:1 metal−peptide complex. However, the 1:1 Cu(II)-OP4 complex is readily decomposed into the Cu(I) ion and peptide (eq 3). This makes it difficult to experimentally study the structural role of tryptophan in the OP4-mediated Cu(II) reduction. Here we have investigated the structure of the 1:1 Cu(II)−OP4 complex by molecular mechanics calculations to get insight into the role of tryptophan.

Figure 8 shows the lowest energy structure among a few hundred sterically possible conformers of the 1:1 Cu(II)-OP4 complex with a Cu(II)−Nτ_4-type coordination. The peptide main chain of OP4 is depicted as a string except for the most C-terminal glycine residue of the third OP unit (Gly-3). Side-chain atoms are shown only for tryptophan and Cu(II)−ligand amino acids. The Cu(II) ion is coordinated by the Nτ atoms of four histidine residues (His-1, His-2, His-3, and His-4) at a distance of 2.02−2.04 Å in a square-planar geometry. In addition, the side-chain carbonyl oxygen of the glutamine residue in the first OP unit (Gln-1) and the main-chain carbonyl oxygen of Gly-3 occupy axial positions at a distance of 2.42−2.43 Å from the metal center to form

a six-coordinate tetragonal geometry (or a square-bipyramidal geometry).

Of four tryptophan residues, two belonging to the third and fourth OP units (Trp-3 and Trp-4) are located far away (~10 Å) from the Cu(II) ion and also from each other. On the other hand, the other two tryptophan residues of the first and second OP units (Trp-1 and Trp-2) gather on one side of the Cu(II) center, where His-2 is coordinating to the Cu(II) ion. The indole ring of Trp-2 is in close contact (2.97 Å) with the Nπ atom of His-2, suggesting a direct interaction between the indole and imidazole rings. Furthermore, the indole N1 atom of Trp-2 is close (2.94 Å) to the indole ring of Trp-1, which is not in direct contact with His-2. The N1 atom of Trp-1, in turn, is exposed to the solvent. Possibly, Trp-1, Trp-2, and His-2 form a path of electron transfer for the reduction of the Cu(II) ion captured by the histidine ligands. It is likely that the OP4-mediated Cu(II) reduction is made possible by the square-planer coordination of four His Nτ atoms, which increases the redox potential of Cu(II) (*52*, *53*), and the close arrangement of two redox-active Trp indole rings around one His ligand, which facilitates electron transfer.

DISCUSSION

The present kinetic assays have revealed that the four tandem repeat of the octapeptide unit (OP4) is an essential requirement for the peptide-mediated reduction of Cu(II) (Figure 3). Shorter peptides OP1, OP2, and OP3 are inactive although each OP unit can bind a single Cu(II) ion at pH $\geq$7.4 (*20*−*25*). The requirement of four OP units is consistent with the structure of the 1:1 Cu(II)−OP4(W→A) complex, which corresponds to the active intermediate of the OP4-mediated Cu(II) reduction and has a Cu(II) ion coordinated by four histidine Nτ atoms [Cu(II)−Nτ_4]. The feasibility of forming the Cu(II)−Nτ_4-type complex may govern the Cu(II) reduction activity of OP4. In other words, any factors that disfavor the formation of the Cu(II)−Nτ_4-type complex would decrease the activity of Cu(II) reduction. OP4 reduces Cu(II) ions most efficiently at pH ~6.5 because only the Nτ−Cu(II) coordination occurs at this pH (Figure 6). At more acidic pH, some histidine residues are protonated to be cationic His^+, and the full coordination of four histidine residues to a single Cu(II) ion is hindered, resulting in a loss of reduction activity (Figures 2 and 7A). At neutral-to-alkaline pH, on the other hand, the peptide main-chain amide nitrogen gains affinity for Cu(II), and each OP unit binds a Cu(II) ion by using a histidine Nπ atom and one or more deprotonated amide nitrogens [Cu(II)−(Nπ, $amide^-$)] (Figures 2 and 7C,D). The Cu(II)−(Nπ, $amide^-$)-type coordination competes with the Cu(II)−Nτ_4-type coordination, and the Cu(II) reduction activity decreases at neutral-to-alkaline pH compared to that at pH ~6.5. The Cu(II) binding mode of OP4 is a key factor that determines its Cu(II) reduction activity.

Molecular mechanics calculations have provided a plausible model for the active intermediate in the Cu(II) reduction by OP4 (Figure 8). According to the model, the Cu(II) ion is coordinated by four Nτ atoms of histidine in a square-planar geometry with two carbonyl oxygen atoms as additional weaker axial ligands. Another characteristic of the model structure is that two of the four tryptophan residues (Trp-1 and Trp-2) are positioned in the vicinity of His-2, one of the Cu(II) ligands, suggesting electron transfer from redox-active tryptophan to Cu(II) via the metal-coordinated histidine residue. A possible mechanism of Cu(II) reduction may be as follows: (1) Trp-2 donates an electron to the Cu(II) ion via His-2. (2) The linkage between the reduced Cu(I) ion and OP4 is weakened because the Cu(I) ion strongly favors four-coordinate tetrahedral or three-coordinate trigonal-planar geometries and does not fit in the square-planar geometry (or the six-coordinate tetragonal geometry) of the Cu(II) coordination (*53*, *54*). The loosened Cu(I) ion may be released from the complex and captured by Cu(I)-specific ligands such as BC. (3) Trp-2 in the cationic radical state extracts an electron from nearby Trp-1. (4) Trp-1, which is exposed to the solvent, is reduced by exogenous reductants in the solution (*55*, *56*). In the present reduction assay, amino acid glycine, which was originally bound to Cu(II), may be one of such exogenous reductants (*57*). The model proposed here accounts for the importance of tryptophan residues in the Cu(II) reduction. The first cycle of the reaction may correspond to the initial burst phase of the Cu(II) reduction and the subsequent cycles to the steady state. The decreased velocity in the steady state compared to that in the initial burst phase may be ascribed to the involvement of the electron transfer process from an exogenous reductant to Trp-1 on returning to the initial state.

PrP has been proposed to play a role in transporting Cu(II) ions from the extracellular to intracellular space through endocytosis of the protein itself (*12*−*14*, *20*, *22*, *28*). Since the octapeptide repeat region of PrP has an ability to bind four Cu(II) ions at extracellular neutral pH but only one Cu(II) ion at endosomal acidic pH, the Cu(II) ions captured in the extracellular space are expected to be released in the endosomal compartment (*18*, *22*, *23*, *28*). The released Cu(II) ions, however, need to be reduced to Cu(I) and transported to the cytoplasm across the endosome membrane for efficient use of the ions. This is because Cu(I), rather than Cu(II), is bound and delivered by copper chaperones to target proteins in the cytoplasmic space and intracellular copper trafficking is made in the reduced Cu(I) form (*29*, *30*). The necessity of Cu(II) reduction in the endosome is consistent with the present finding that Cu(II) ions are readily reduced by the octapeptide repeat region of PrP, in particular in endosomal acidic environments. Although PrP reduces only one Cu(II) ion at a time, all of the Cu(II) ions that are captured on the plasma membrane surface and released in the endosome may be, one by one, reduced to Cu(I) by PrP and transported to copper chaperones outside the endosome. Thus, the rate of Cu(II) reduction is important for efficient use of the captured Cu(II) ions, and we have shown that the reduction is most efficiently carried out at acidic endosomal pH. It is strongly suggested that PrP plays an important role in cellular copper uptake by capturing and reducing Cu(II) ions.

Transportation of copper across the endosome membrane, on the other hand, may be performed by the Cu(I)-specific transporter Ctr1, which is also a membrane-bound protein and is endocytosed upon exposing the cell to high copper concentrations as was observed for PrP (*58*, *59*). The coexistence of PrP and Ctr1 in an endosome is not unlikely to happen because both proteins are internalized by clathrin-mediated endocytosis that takes place at specific regions of the plasma membrane called clathrin-coated pits (*59*, *60*). It

is highly probable that PrP reduces the released Cu(II) ions in the endosome and the reduced Cu(I) ions are transported by Ctr1 to copper chaperones in the cytoplasm. The coupling of PrP-mediated Cu(II) reduction and Ctr1-mediated Cu(I) transport may also occur on the plasma membrane surface, where both proteins are mainly localized. PrP has an ability to reduce the Cu(II) ions even at extracellular neutral pH (Figure 2), and the Cu(I) transport activity of Ctr1 is also significant at neutral pH (*61*). Metalloreductases coupled with Ctr1 have been identified for yeast Ctr1 but not for mammalian Ctr1 (*29*). PrP may be a copper reductase coupled with mammalian Ctr1.

REFERENCES

1. Prusiner, S. B. (1991) Molecular biology of prion diseases, *Science 252*, 1515−1522.
2. Mobley, W. C., Neve, R. L., Prusiner, S. B., and McKinley, M. P. (1988) Nerve growth factor increases mRNA levels for the prion protein and the β-amyloid protein precursor in developing hamster brain, *Proc. Natl. Acad. Sci. U.S.A. 85*, 9811−9815.
3. Stahl, N., Borchelt, D. R., Hsiao, K., and Prusiner, S. B. (1987) Scrapie prion protein contains a phosphatidylinositol glycolipid, *Cell 51*, 229−240.
4. Schätzl, H. M., Da Costa, M., Taylor, M., Cohen, F. E., and Prusiner, S. B. (1995) Prion protein gene variation among primates, *J. Mol. Biol. 245*, 362−374.
5. Locht, C., Chesebro, B., Race, R., and Keith, J. M. (1986) Molecular cloning and complete sequence of prion protein cDNA from mouse brain infected with the scrapie agent, *Proc. Natl. Acad. Sci. U.S.A. 83*, 6372−6376.
6. Riek, R., Hornemann, S., Wider, G., Billeter, M., Glockshuber, R., and Wüthrich, K. (1996) NMR structure of the mouse prion protein domain PrP(121−321), *Nature 382*, 180−182.
7. James, T. L., Liu, H., Ulyanov, N. B., Farr-Jones, S., Zhang, H., Donne, D. G., Kaneko, K., Groth, D., Mehlhorn, I., Prusiner, S. B., and Cohen, F. E. (1997) Solution structure of a 142-residue recombinant prion protein corresponding to the infectious fragment of the scrapie isoform, *Proc. Natl. Acad. Sci. U.S.A. 94*, 10086−10091.
8. Donne, D. G., Viles, J. H., Groth, D., Mehlhorn, I., James, T. L., Cohen, F. E., Prusiner, S. B., Wright, P. E., and Dyson, H. J. (1997) Structure of the recombinant full-length hamster prion protein PrP(29−231): the N terminus is highly flexible, *Proc. Natl. Acad. Sci. U.S.A. 94*, 13452−13457.
9. Zahn, R., Liu, A., Lührs, T., Riek, R., Schroetter, C., García, F. L., Billeter, M., Calzolai, L., Wider, G., and Wüthrich, K. (2000) NMR solution structure of the human prion protein, *Proc. Natl. Acad. Sci. U.S.A. 97*, 145−150.
10. Prusiner, S. B. (1997) Prion diseases and the BSE crisis, *Science 278*, 245−251.
11. Prusiner, S. B. (1998) Prions, *Proc. Natl. Acad. Sci. U.S.A. 95*, 13363−13383.
12. Pauly, P. C., and Harris, D. A. (1998) Copper stimulates endocytosis of the prion protein, *J. Biol. Chem. 273*, 33107−33119.
13. Brown, D. R. (1999) Prion protein expression aids cellular uptake and veratridine-induced release of copper, *J. Neurosci. Res. 58*, 717−725.
14. Brown, L. R., and Harris, D. A. (2003) Copper and zinc cause delivery of the prion protein from the plasma membrane to a subset of early endosomes and the Golgi, *J. Neurochem. 87*, 353−363.
15. Brown, D. R., Qin, K., Herms, J. W., Madlung, A., Manson, J., Strome, R., Fraser, P. E., Kruck, T., von Bohlen, A., Schulz-Schaeffer, W., Giese, A., Westway, D., and Kretzschmar, H. (1997) The cellular prion protein binds copper in vivo, *Nature 390*, 684−687.
16. Brown, D. R. (2003) Prion protein expression modulates neuronal copper content, *J. Neurochem. 87*, 377−385.
17. Hornshaw, M. P., McDermott, J. R., and Candy, J. M. (1995) Copper binding to the N-terminal tandem repeat regions of mammalian and avian prion protein, *Biochem. Biophys. Res. Commun. 207*, 621−629.
18. Stöckel, J., Safar, J., Wallace, A. C., Cohen, F. E., and Prusiner, S. B. (1998) Prion protein selectively binds copper(II) ions, *Biochemistry 37*, 7185−7193.
19. Miura, T., Hori-i, A., and Takeuchi, H. (1996) Metal-dependent α-helix formation promoted by the glycine-rich octapeptide region of prion protein, *FEBS Lett. 396*, 248−252.
20. Miura, T., Hori-i, A., Mototani, H., and Takeuchi, H. (1999) Raman spectroscopic study on the copper(II) binding mode of prion octapeptide and its pH dependence, *Biochemistry 38*, 11560−11569.
21. Aronoff-Spencer, E., Burns, C. S., Avdievich, N. I., Gerfen, G. J., Peisach, J., Antholine, W. E., Ball, H. L., Cohen, F. E., Prusiner, S. B., and Millhauser, G. L. (2000) Identification of the Cu^{2+} binding sites in the N-terminal domain of the prion protein by EPR and CD spectroscopy, *Biochemistry 39*, 13760−13771.
22. Whittal, R. M., Ball, H. L., Cohen, F. E., Burlingame, A. L., Prusiner, S. B., and Baldwin, M. A. (2000) Copper binding to octarepeat peptides of the prion protein monitored by mass spectrometry, *Protein Sci. 9*, 332−343.
23. Qin, K., Yang, Y., Mastrangelo, P., and Westaway, D. (2002) Mapping Cu(II) binding sites in prion proteins by diethyl pyrocarbonate modification and matrix-assisted laser desorption ionization-time of flight (MALDI-TOF) mass spectrometric footprinting, *J. Biol. Chem. 277*, 1981−1990.
24. Viles, J. H., Cohen, F. E., Prusiner, S. B., Goodin, D. B., Wright, P. E., and Dyson, H. J. (1999) Copper binding to the prion protein: structural implications of four identical cooperative binding sites, *Proc. Natl. Acad. Sci. U.S.A. 96*, 2042−2047.
25. Garnett, A. P., and Viles, J. H. (2003) Copper binding to the octarepeats of the prion protein. Affinity, specificity, folding, and cooperativity: insights from circular dichroism, *J. Biol. Chem. 278*, 6795−6802.
26. Hornshaw, M. P., McDermott, J. R., Candy, J. M., and Lakey, J. H. (1995) Copper binding to the N-terminal tandem repeat region of mammalian and avian prion protein: structural studies using synthetic peptides, *Biochem. Biophys. Res. Commun. 214*, 993−999.
27. Jackson, G. S., Murray, I., Hosszu, L. L., Gibbs, N., Waltho, J. P., Clarke, A. R., and Collinge, J. (2001) Location and properties of metal-binding sites on the human prion protein, *Proc. Natl. Acad. Sci. U.S.A. 98*, 8531−8535.
28. Burns, C. S., Aronoff-Spencer, E., Dunham, C. M., Lario, P., Avdievich, N. I., Antholine, W. E., Olmstead, M. M., Vrielink, A., Gerfen, G. J., Peisach, J., Scott, W. G., and Millhauser, G. L. (2002) Molecular features of the copper binding sites in the octarepeat domain of the prion protein, *Biochemistry 41*, 3991−4001.
29. Harrison, M. D., Jones, C. E., and Dameron, C. T. (1999) Copper chaperones: function, structure and copper-binding properties, *J. Biol. Inorg. Chem. 4*, 145−153.
30. Rosenzweig, A., and O'Halloran, T. V. (2000) Structure and chemistry of the copper chaperone proteins, *Curr. Opin. Chem. Biol. 4*, 140−147.
31. Ruiz, F. H., Silva, E., and Inestrosa, N. C., (2000) The N-terminal tandem repeat region of human prion protein reduces copper: role of tryptophan residues, *Biochem. Biophys. Res. Commun. 269*, 491−495.
32. Smith, G. F., and Wilkins, D. H. (1953) New colorimetric reagent specific for copper: determination of copper and iron, *Anal. Chem. 25*, 510−511.
33. Multhaup, G., Schlicksupp, A., Hesse, L., Beher, D., Ruppert, T., Masters, C. L., and Beyreuther, K. (1996) The amyloid precursor protein of Alzheimer's disease in the reduction of copper(II) to copper(I), *Science 271*, 1406−1409.
34. Huang, X., Cuajungco, M. P., Atwood, C. S., Hartshorn, M. A., Tyndall, J. D., Hanson, G. R., Stokes, K. C., Leopold, M., Multhaup, G., Goldstein, L. E., Scarpa, R. C., Saunders, A. J., Lim, J., Moir, R. D., Glabe, C., Bowden, E. F., Masters, C. L., Fairlie, D. P., Tanzi, R. E., and Bush, A. I. (1999) Cu(II) potentiation of Alzheimer Aβ neurotoxicity, *J. Biol. Chem. 274*, 37111−37116.
35. Kirkpatrick, S., Gelatt, C. D., and Vecchi, M. P. (1983) Optimization by simulated annealing, *Science 220*, 671−680.
36. Shi, S., Yan, L., Yang, Y., Fisher-Shaulsky, J., and Thacher, T (2003) An extensible and systematic force field, ESFF, for molecular modeling of organic, inorganic, and organometallic systems, *J. Comput. Chem. 24*, 1059−1076.
37. Frieden, C. (1979) Slow transitions and hysteretic behavior in enzymes, *Annu. Rev. Biochem. 48*, 471−489.

38. Neet, K. E., and Ainslie, G. R., Jr. (1980) Hysteretic enzymes, *Methods Enzymol. 64*, 192−226.
39. DeFelippis, M. R., Murthy, C. P., Broitman, F., Weinraub, D., Faraggi, M., and Klapper, M. H. (1991) Electrochemical properties of tyrosine phenoxy and tryptophan indolyl radicals in peptides and amino acid analogues, *J. Phys. Chem. 95*, 3416−3419.
40. Jovanovic, S. V., Steenken, S., and Simic, M. G. (1991) Kinetics and energetics of one-electron-transfer reactions involving tryptophan neutral and cation radicals, *J. Chem. Phys. 95*, 684−687.
41. Fersht, A. (1977) *Enzyme Structure and Mechanism*, Freeman, New York.
42. Pastra-Landis, S. C., Evans, D. R., and Lipscomb, W. N. (1978) The effect of pH on the cooperative behavior of aspartate transcarbamylase from *Escherichia coli*, *J. Biol. Chem. 253*, 4624−4630.
43. Licata, V. J., and Allewell, N. M. (1997) Is substrate inhibition a consequence of allostery in aspartate transcarbamylase?, *Biophys. Chem. 64*, 225−234.
44. Miura, T., Suzuki, K., Kohata, N., and Takeuchi, H. (2000) Metal binding modes of Alzheimer's amyloid beta-peptide in insoluble aggregates and soluble complexes, *Biochemistry 39*, 7024−7031.
45. Takeuchi, H. (2003) Raman structural markers of tryptophan and histidine side chains in proteins, *Biopolymers 72*, 305−317.
46. Ashikawa, I., and Itoh, K. (1979) Raman spectra of polypeptides containing L-histidine residues and tautomerism of imidazole side chain, *Biopolymers 18*, 1859−1876.
47. Miura, T., Satoh, T., Hori-i, A., and Takeuchi, H. (1998) Raman marker bands of metal coordination sites of histidine side chains in peptides and proteins, *J. Raman Spectrosc. 29*, 41−47.
48. Hashimoto, S., Ono, K., and Takeuchi, H. (1998) UV Raman scattering from metal-coordinating histidine residues in Cu,Zn-superoxide dismutase, *J. Raman Spectrosc. 29*, 969−975.
49. Miura, T., Satoh, T., and Takeuchi, H. (1998) Role of metal-ligand coordination in the folding pathway of zinc finger peptides, *Biochim. Biophys. Acta 1384*, 171−179.
50. Tasumi, M. (1979) Interaction of metal ions with peptides in aqueous medium as studied by infrared and Raman spectroscopy, in *Infrared and Raman Spectroscopy of Biological Molecules* (Theophanides, T. M., Ed.) pp 225−240, D. Reidel Publishing Co., Dordrecht.
51. Tsangaris, J. M., Chang, J. W., and Martin, R. B. (1969) Ultraviolet circular-dichroism of cupric and nickel ion complexes of amino acids and peptides, *J. Am. Chem. Soc. 91*, 726−731.
52. Addison, A. W. (1989) Is ligand topology an influence on the redox potentials of copper complexes?, *Inorg. Chim. Acta 162*, 217−220.
53. Rorabacher, D. B. (2004) Electron transfer by copper centers, *Chem. Rev. 104*, 651−697.
54. Ambundo, E. A., Deydier, M.-V., Grall, A. J., Aguera-Vega, N., Dressel, L. T., Cooper, T. H., Heeg, M. J., Ochrymowycz, L. A., and Rorabacher, D. B. (1999) Influence of coordination geometry upon copper(II/I) redox potentials. Physical parameters for twelve copper tripodal ligand complexes, *Inorg. Chem. 38*, 4233−4242.
55. Aubert, C., Vos, M. H., Mathis, P., Eker, A. P., and Brettel, K. (2000) Intraprotein radical transfer during photoactivation of DNA photolyase, *Nature 405*, 586−590.
56. Byrdin, M., Sartor, V., Eker, A. P., Vos, M. H., Aubert, C., Brettel, K., and Mathis, P. (2004) Intraprotein electron transfer and proton dynamics during photoactivation of DNA photolyase from E. coli: review and new insights from an "inverse" deuterium isotope effect, *Biochim. Biophys. Acta 1655*, 64−70.
57. Dean, R. T., Fu, S., Stocker, R., and Davies, M. J. (1997) Biochemistry and pathology of radical-mediated protein oxidation, *Biochem. J. 324*, 1−18.
58. Kuo, Y. M., Zhou, B., Cosco, D., and Gitschier, J. (2001) The copper transporter CTR1 provides an essential function in mammalian embryonic development, *Proc. Natl. Acad. Sci. U.S.A. 98*, 6836−6841.
59. Petris, M. J., Smith, K., Lee, J., and Thiele, D. J. (2003) Copper-stimulated endocytosis and degradation of the human copper transporter, hCtr1, *J. Biol. Chem. 278*, 9639−9646.
60. Harris, D. A. (2003) Trafficking, turnover and membrane topology of PrP, *Br. Med. Bull. 66*, 71−85.
61. Lee, J., Pena, M. M., Nose, Y., and Thiele, D. J. (2002) Biochemical characterization of the human copper transporter Ctr1, *J. Biol. Chem. 277*, 4380−4387.

BI0501784